This is the Author Accepted Manuscript (postprint) of:
Terrado et al., 2011, J. Phys. Chem. C , 115, 9312–9319
https://doi.org/10.1021/jp101351y

Modifying the Heat Transfer and Capillary Pressure of Loop Heat Pipe Wicks with Carbon Nanotubes

E. Terrado, R. Molina, E. Natividad, M. Castro, P. Erra, D. Mishkinis, A. Torres, M. T. Martínez*

*Corresponding author: M. T. Martínez (mtmartinez@icb.csic.es)

Instituto de Carboquímica (CSIC), Zaragoza, Spain

Chemical and Biological Nanotechnology Department, Institute of Chemical and Environmental Chemistry of Barcelona (CSIC), Spain

Instituto de Ciencia de Materiales de Aragón (CSIC–Universidad de Zaragoza), Zaragoza, Spain

Iberespacio, Fuencarral 123, 5a P 28010 Madrid, Spain

Abstract

Porous material is a critical component in the loop heat pipe (LHP) device, the efficiency of which depends on the thermal conductivity of the wick and its capillary capacity. A new bilayer wick based on ceramic material and carbon nanotubes in the outer surface has been designed. The thermal conductivity and capillary pressure of the surface of a ceramic LHP wick prototype have been modified by growing multiwalled carbon nanotubes (MWCNTs). The presence of a thin layer of MWCNTs increased the thermal conductivity of wick specimens between 18.87 and 26.42% for temperatures ranging from -50 to 50 ºC. The thermal conductivity of the grown MWCNTs calculated considering a mean layer thickness of 5 μm was 59 W/mK. The effective pore diameter of zircon ceramic wicks decreased from 0.54 to 0.31 μm leading to an important increase in capillary pressure. The maximum heat transfer capacity and thermal resistance of the designed by-layer wick have been determined. The presence of carbon nanotubes decreases the thermal resistance and enabled the enhancement of the thermal and porous characteristics of the wicks in a promising way so as to optimize their performance as LHPs wicks.

INTRODUCTION

The combination of structure, topology, and dimensions of CNTs creates a host of unparalleled physical properties that have boosted the exploration of their use in diverse applications, ranging from nanoscale circuits for beyond silicon based metal- oxide-semiconductor era electronics,[1-3] to low-voltage cold- cathodes, field-emission displays,4 agents for drug delivery,5,6 light-emitting devices,[7,8] electrical interconnects,[9] and chemical/ biological sensors.[10,11]

One of the most outstanding properties of CNTs is their high thermal conductivity, surpassing values seen with diamonds owing to their strong carboncarbon chemical bonding.[12] Single-walled carbon nanotubes (SWCNTs) show ballistic con- duction at low temperatures leading to quantization in heat transport, even in the presence of defects. The heat-transport behavior changes from quasi ballistic to diffusive at temperatures above room temperature. The heat flow in MWCNTs, as in the case of SWNTs, is predominantly carried by phonons.[13] Unlike SWNTs, large-diameter MWCNTs cannot be regarded as simple one-dimensional phonon systems. They exhibit complex heat-transport phenomena because of interwall interaction. To observe the quantizationofMWCNTsthermal conductance, itisnecessary to lower the temperature to T ∼1 K for typical MWCNTs.[13]

However, the high thermal conductivity of CNTs is diminished by defects (e.g., a vacancy defect, an isotope impurity, or a StoneWales defect) generated during CNT synthesis, or by artificial operations such as ion/electron irradiation. Although the experimental reported values are lower than the theoretical value, they are still comparable to the thermal conductivity of the highest-purity graphite.[14,15] Thermal conductivity reported for millimeter-sized carbon nanotube mats is in the order of 10300 W/mK[16] and more recently between 40 to 343 for MWCNTs and 600 for SWCNTs.[17] Structural defects such as atomic vacancies and array misalignments induce strong intertube couplings of phonons in different walls, reducing the thermal conductivity.[18]

On account of their high thermal conductivity, the heat transport in CNTs has attracted much attention from both theoretical[19,20] and experimental points of view.[12,21] Their high thermal conductivity has very recently been exploited to develop a CNT-based heat-removal device that efficiently dissipates the heat generated by an integrated circuit,[22] in

thermal heat sink applications,[23] film heaters,[24] and in applications as thermal interface materials.

In ceramics, studies on CNT-aluminum nitride[29] and silicon nitride composites[30] have been conducted for a variety of structural and mechanical applications and have shown thermal properties enhancement as compared with the pristine matrix. Padture,[31] has reported a discussion and analysis of recent developments in these composites. Application of carbon nanostructures in thermal circuit systems and adapters of a variety of materials including ceramics have been reported by Anttoniette et al.[32] However, in our knowledge neither carbon nanotubes nor any other nanostructured carbon have been applied in loop heat pipes (LHPs) refrigeration systems so far.

In the present work, a small-scale zircon wick LHP prototype with a bilayer design has been prepared. CNTs were grown on the wick surface to increase the surface thermal conductivity and capillary pressure on the outer ceramic surface with the aim of fitting the technical requirements of a prototype LHP wick.

LHPs are two-phase heat transfer devices that utilize the evaporation and condensation of a working fluid to transfer heat, and the capillary forces generated in porous wicks to circulate the fluids. Fluid-in-liquid phase is vaporized in the evaporator, close to the units where heat is generated. Vapor is then driven to the condenser where it is condensed again and returned to the evaporator. The pressures necessary for driving the vapor and inducing the circulation of the fluid, generally ammonia, through the system are a consequence of the capillary forces from the porous material used to make the wick. Porous material is a critical component in the LHP device, the efficiency of which depends on the thermal conductivity of the wick, its capillary capacity, and its mechanical features.

The choice of wick material and its physical properties, such as pore size, porosity, permeability, and thermal conductivity has considerable effect on the operational characteristics of the wick. The capillary structure is usually made of plastic or metal. Plastic wicks made of polypropylene, Teflon, and polyethylene[33] present very low thermal conductivity, which is desirable for efficient LHP operation to avoid vapor bubbles appearance on the liquid part of the wick, which could discontinue the pumping, but they have poor capillary pumping characteristics due to poor wet- ability. Using low

thermal conductivity wicks, problems associated with high conductivity wicks like the parasistic heat, the heat leak from evaporator to the compensation chamber and the instability at the LHPs start up are overcome. However, in addition to thermal management the capillary pressure is very important to get the fluid to pump in the right way in the system. Other problems often associated with plastic wicks are the rather limited operational temperature range and the plastic wick compatibility with working fluids. Moreover, at present time there are not plastic wicks on the market with average pore size less than 34 μm (with porosity value more than 50%).

Sintered powder metallic (stainless steel, Ti, Ni, Cu, and so forth) wicks are widely used as capillary pumps in loop heat pipes nowadays due to an excellent pumping capacity,[34] relatively high permeability, and porosity (usually 5060% but up to 75%). However, relatively high thermal conductivity of the wicks (10100 W/mK) leads to the problems outlined before of low power and transient regimes of LHP operation caused by intensive boiling process in central channel of metal wicks.

The porous structure in the evaporator serves as (i) a liquid capillary pump, to provide constant fluid flow in the loop, and (ii) a vapor generator, to remove the heat from a source by latent heat of vaporization. Usually, a single wick has those two functions in inverted meniscus evaporators. However, this approach is not optimal. The small average pore size (several micrometers) capillary structure with low thermal conductivity (to avoid vapor bubbles appearance on the liquid part of the wick which could discontinue the pumping) is required to support the liquid circulation in the loop. But the structure with a developed surface and high effective thermal conductivity is preferable in a heat input region of heat loop. Designers of LHPs with the inverted meniscus evaporator have tried to manufacture special wicks with two different porous structures[35,36] but the manufacturing pro- cess is very complex and expensive. Notwithstanding that biporous wick[35] and biporous layer[36] provide significant enhance of LHP performance (for instance, the biporous layer evaporator has heat exchange coefficients about 3070% higher than uniporous evaporator with the decreasing of the LHP start-up heat load in 23 times).

The proposed bilayer design in this paper has two separate structures, which are responsible for the following two different functions: (1) Mass transfer structure (MTS),

which is working as a capillary pump. It is ceramic cylinder. (2) Heat transfer structure (HTS). It is the CNTs layer. The second enhanced evaporation heat transfer structure is needed for the efficient liquid delivery to an extended evaporating surface and following vapor evacuation through low hydraulic resistance developed system of channels to the LHP condenser. Figure 1 shows a simplified diagram of a LHP. MTS has to be a structure with low-thermal conductance, high permeability, and good capillary suction (small average effective diameter of a pore/channel and high wetability). Actually, the wick main parameters such as porosity, permeability, and average pore size are interconnected. In practice, the wicks with average pore size less than 3020 μm are required. Thus, ceramic wicks have certain advantages over metallic wicks as MTS due to much lower thermal conductivity values (0.11 W/mK) HTS has to support high heat rate and flux density with small temperature difference between a heat source and saturated vapor of working fluid.

Selective CNT growth on the outer ceramic surface will allow pore size reduction, making cooling liquid drive easier by means of the higher capillary pressure created. Simultaneously CNTs would increase the thermal conductivity on the surface so it reduces temperature difference between the heat source and evaporating fluid, which finally would lead to the increase of the LHP efficiency. It is foreseeable that the use of this bilayer design would lead the enhancement of evaporation heat transfer coefficient compared with the raw ceramic wick and compared with the metallic wicks, to the reduction of the parasitic heat, the heat leak from evaporator to the compensation chamber, and the instability at the LHPs start-up

Consequently, CNTs grown on the ceramic surface are expected to lead to an enhanced performance of the base ceramic material for application in LHPs

EXPERIMENTAL METHODS

CNTs were grown over small wick specimens (2.5 cm length, Figure 1 right Supporting Information) of three different cera- mics, zircon stabilized with yttrium oxide (TOSOH 3ZYSE) (IVF, Industrial Research and Development Corporation, Swedish Ceramin Institute), cordierite (Ad-Teramics Wick), and mullite (OI Filtration Ltd. & Ceramin Engineers) The following different conditions for the MWCNTs growth were tested: NiMo and CoMo catalysts supported on magnesium oxide using methane (100 mL/min)

as carbon precursor at 1000 C and reaction times of 30, 10, 2, and 1 min. Conditions for metallic salts (Fe(NO3)3, 9H2O, and Ni(NO3)2 3 6H2O) as a catalyst wereatconcentrations of50, 100, and150 mM, temperatures of 750, 800, 850, and 900 C, reaction times of 5, 7.5, and 10 min and acetylene as carbon precursor. Attending to the MWCNTs coverage and the increase of thermal conductivity, zircon ceramics showed the best perfor- mance and MWCNTs were grown over whole zircon wicks (Figure 1 left Supporting Information). The wick consisted of a zircon cylinder (length = 15 cm, outer diameter = 2.54 cm, inner diameter = 1 cm) with machined longitudinal grooves which behaving as vapor removal channels. The zircon wicks were washed with acetone and isopropyl alcohol by sonication and after drying were coated with the catalyst. The ceramic wicks were immersed in iron nitrate solution in ethanol (0.1 M) for 24 h to impregnate them with catalyst. The Fe catalyst-coated ceramics were then placed in the center of a quartz tubular furnace on a horizontal rotisserie-like boat that was specially designed to hold the ceramic cylinder and keep the outer ceramic surface in contact with the gas environ- ment inside the reactor (Figure 1 right Supporting Information). To obtain Fe-catalyst nanoparticles with the desired nanosize and activity for the CNT nucleation, a thermal pretreatment process was carried out under nitrogen atmosphere for 25 min followed by an ammonia reductive treatment for 5 min. CNTs were grown at 850 C for 20 min using acetylene at atmospheric pressure and the reactor was cooled down to room temperature under nitrogen. The resulting CNTs were characterized by scanningelectronmicroscopy(HitachiS-3400N) andtransmission electron microscopy (JEOL-200FXII). Porosity of pristine zir- con wicks and those with CNTs was characterized by mercury porosimetry and by nitrogen BrunauerEmmettTeller (BET) adsorption isotherms and compared with the values for the original wicks. Thermal conductivity was determined with a commercial setup(Termis Ltd.)thatprovided thermalconductance(K) values by means of a longitudinal steady-state method. In this setup, the heat interchange between the sample and surroundings was minimized by the use of vacuum conditions and a lateral radiation shield. The measuring process consists of the establishment of a temperature difference between the ends of a sample with well-defined geometry and the measurement of the heat power required to maintain such a temperature difference in stationary conditions. The thermal conductance is then

calculated from the ratio of the heat power and the temperature difference, and thermal conductivity data can be obtained from the expression κ = K 3 L/A, where L and A are the length and the cross-section of the sample, respectively. Further details of the setup, measur- ing process, and data treatment have been described previously.37 Prismatic samples of about 8 mm length were measured with and without the CNT layer. The thermal conductivity calculation was performed considering the CNT and wick structures in parallel configurations (see Supporting Information). Contact angle measurements were carried out by two distinct methods. Samples exhibiting capillary rise phenomena were measured by determining the amount of liquid absorbed by the sample as a function of time according to the Washburn method. For hydrophobic surfaces, where capillary rise phe- nomena do not occur, advancing contact angles were determined by means of the Wilhelmy method. Contact angle measurements were carried out in a KSV Sigma 70 electrobalance by determin- ing the amount of liquid absorbed by the sample as a function of the time using decane and water as reference liquids. The Washburn equation relates the amount of liquid that penetrates into a porous structure as a function of time with liquid physical parameters (density, surface tension, and viscosity), sample geometric structure (related with the pore distribution and connection between them) and solidliquid contact angle [eq 1][38]

$$m^2 = c\frac{\rho_L^2 \gamma_L \cos\theta}{2\eta_L} t$$

Here m is the liquid mass, c is the capillary constant related with the geometric structure, FL is the liquid density, γL is the liquid surface tension, θ is the solidliquid contact angle, ηL is the liquid viscosity, and t is the measurement time. The capillary constant was determined using decane as the complete wetting liquid. The effective pore radius (reff) can be obtained taking into account the material porosity (ε) and the geometric area of the sample (A) by means of eq 2[39,40]

$$c = \frac{1}{2}(A\varepsilon)^2 r_{eff}$$

When applying the Wilhelmy method, advancing contact angles were calculated from dynamic wetting force (Fw) measurements. Samples were scanned at a velocity of 0.5 mm/min in both advancing and receding modes.[41] The detachment of the MWCNTs from the surface of the ceramic could lead to problems in the system during the evaporation condensation cycles due to the accumulation of the CNTs in certain zones provoking pore plugging. The adhesion of the MWCNTs was tested by applying several stirring and ultrasonic treatments of different intensity to CNT-coated zircon pieces in aqueous solution (i) mechanical stirring at 400 and 800 rpm for 30 to 120 min, (ii) ultrasonic treatment (US) at 50 Hz for 5 min (iii) US treatment followed by mechanical stirring. After the treatments, the ceramics were dried at 110 C and observed with scanning electron microscopy (SEM). Characteristics of the wicks were experimentally investigated. A schematic diagram of the setup is presented on Figure 2 Supporting Information. The investigated wick (2) was hydraulically connected by stainless steel screen mesh with secondary wick (1) and with water (8). The heat has been applied to the wick 2 by heater 4 with steps of 10 W. The temperature difference between the Al saddle and the average vapor temperature in the grooves was registered automatically every 10 s. Water was evaporated into the ambient. Temperature (∼40 C) and liquid level of water in the container 8 was maintained constant during the experiment. Two main characteristics of the wick, maximum heat transfer capacity and thermal resistance (ratio of tempera- ture difference between temperature of Al interface and vapor in the grooves to applied power), were determined from the experiment.

RESULTS AND DISCUSSION

The zircon wick raw material had a porosity of 48%, pore diameters ranging from 0.5 to 7 μm, and a thermal conductivity ranking from 0.57 to 0.637 W/mK between 50 and 50 C. BET surface area (Table 1) was very low due to the fact that most of the original pores of the ceramic used (determined by mercury porosimetry) were in the macropore range (>50 nm). The growth of CNTs on the ceramic slightly increased the BET surface area, Table 1, due to the development of certain degree of microporosity in the ceramic surface. SEM micrographs, Figure 2, show a dense growth of CNTs with diameters in the

range of 6080 nm, covering the entire outer porous surface of the wick ceramic. The high growth density enabled a certain degree of CNT alignment perpendicular to the tube wall. Moreover, transmission electron microscopy (TEM) studies revealed multiwalled nanotubes (MWCNTs) grew from a base-growth mechanism with a bamboolike structure.[42] The thermal conductivity dependence on the temperature for the pristine zircon ceramic (zircon) and the zircon with MWCNTs (zircon/CNTs) is plotted in Figure 3. The observed increase in the bulk thermal conductivity of the nanocomposite in relation to the ceramic without CNTs is in the range of 19-26% for temperatures between 50 C and 50 C. From these data and considering the cross-section and CNT-layer thickness of the measured zircon/CNTs specimen, the thermal conductivity of the growth MWCNTs can be estimated taking into consideration the measuring method. For zircon/CNTs, the temperature gradient is established parallel to the prism faces covered with CNTs. In this configuration, the overall heat power transferred by conduction is the sum of the power conducted by

both the zircon substrate and the CNT layer, which act as independent heat paths. Then, the thermal conductance value of zircon/CNTs, K, is as well the sum of the individual values, Kz KCNT, as K is the ratio of the heat power and the temperature difference, which is the same for both parts. The thermal conductivity of zircon/CNTs, zircon, and CNTs are, respectively, κ = K 3 L/A, κz = Kz 3 L/Az and κCNT = Kz 3 L/ACNT where L is the specimen length, and A, Az, and ACNT are the cross-section of zircon/CNTs, zircon, and CNTs, respectively, with A = Az ACNT. Substituting in K = Kz KCNT, then, κ = fz 3 κz fCNT 3 κCNT, where fz and fCNT are the cross-section fractions of zircon and CNTs, respectively, within the zircon/ CNTs specimen. Assuming a uniform covering of CNTs and an average layer thickness of 5 μm, as estimated from SEM images, an average κCNT of 59 W/mK was obtained. This thermal conductivity value is in the range of experimental thermal conductivity data reported by Yan et al.[17] The microscopic alignment of the MWCNTs does not provide a macroscopic alignment owing to the pore geometry of zircon leading to lower thermal conductivity values than when the CNTs grow perfectly aligned on flat surfaces. Figure 4 shows the decane absorption curves corresponding to the pristine ceramic zircon and the ceramic coated with CNTs. The decrease in the rate of decane absorption in the CNT-coated zircon

reflects the effect of the decrease on the mean pore radius. Table 1 shows the capillary constant and effective pore radius calculated from the absorption curve in decane according to eq 1 and 2. The absorption curves in water (Figure 3 Supporting Information) showed that the CNT-coated zircon only absorbs a small quantity of water, demonstrating the hydrophobic char- acter of the CNT coating. Taking into account the previously determined capillary constant and applying the eq 1 to the linear region of water absorption curve, the calculated water contact angle for the zircon is 46. The water contact angle obtained is in accordance with values previously reported for zircon materials taking into account the stabilizer (6674)[43] and sample rough- ness (2553).[44] To evaluate the wetting properties of the CNTs grown on the zircon ceramic, contact angle hysteresis cycles, according to the Wilhelmy method, were determined in zircon coated with CNTs. The adhesion tension (F/L) hysteresis cycle evidenced the hydrophobic behavior of the CNTs coating the ceramic zircon (Figure 4 Supporting Information). The advancing adhesion tension values stabilized at 3 mm of immersion depth and then remained constant until 5 mm (F/L ≈50 mN/m). In the receding mode, the adhesion tension values have similar values to those corresponding to the advancing mode. The corresponding advancing and receding contact angles were 135.2 and 135.0, respectively, exhibiting a contact angle hysteresis below 1. Nanostructured aligned CNTs can exhibit a high water contact angle, even higher than 150. Water contact angle on aligned carbon nanotubes depends on the density, alignment, and surface chemistry of carbon nanotubes grown via different methods. Individual CNT have an intrinsic contact angle below 90. However, air can be easily trapped between the droplet and the surface at the very beginning of water contact, forming a typical hydrophobic composite surface (CassieBaxter regime). Then nanostructured aligned CNTs can exhibit a high water contact angle, even higher than 150, although this behavior can only be observed at the very beginning of water contact.[45,46] When a water drop is deposited on the aligned CNT, water percolation occurs as a result of capillary forces. It has been suggested that the competition between the nanotube's flexibility and the intense capillary force acting on them can bend the nanotubes into bundles, destroying completely their alignment.[45] The small amount of water absorbed during the Washburn method experiment (Figure 3 Supporting In- formation) suggests that the water percolation effect in the CNT's coated

zircon is not significant and supports the low water contact angle hysteresis observed. This could explain the small amount of water absorbed during the Washburn method experiment (Figure 3 Supporting Information). The contact angle determined by the Wilhelmy method for the CNTs grown on zircon is slightly lower that other reported for aligned carbon nanotubes (160).[47] It is suggested that the water contact angle (135) observed here reflects both the microstructure of the ceramic zircon and the nanostructure of the aligned carbon nanotubes.

The reduction in the effective pore diameter increases the capillary pressure that is inversely proportional to the effective pore diameter as given by the Young Laplace equation[48]

$$\Delta P_{CAP}\max = \frac{2\gamma_L \cos\theta}{r_{eff}}$$

The contact angle in ammonia, which is the refrigeration liquid to be used in the LHP prototype, behaves in a similar way to decane when involved in a capillary process. Therefore it is foreseeable that the contact angle will approach to 0 with ammonia. Assuming complete wetting and zero contact angle, the decrease in the effective pore diameter by 42% leads to the increase of the capillary pressure in decane from 90 to 150 kPa. The surface tension of ammonia at 11.1 C is 23.4 mN/m.49 This value is similar to the surface tension of decane, 23.9 mN/m making it foreseeable that the capillary pressure of ammonia in the wick will be similar to the decane. This increase in capillary pressure in decane together with the increase in surface heat transfer enables improved performance to be foreseen for MWCNT-covered zircon wicks in LHPs. The capillary pressure values calculated here are higher that those reported for monoporous nickel and monoporous and biporous copper wicks reported by Singh et al.[34] and these values seem to fulfill the LHP serviceability condition[50] for conventional heat pipes to generate enough capillary pressure to keep the working fluid in continuous circulation. This condition can be stated mathematically as follows

$$\Delta P_{CAP} \geq \Delta P_v + \Delta P_l + \Delta P_g$$

Being ΔPCAP the generated capillary pressure, ΔPv and ΔPl are pressure losses during the motion of the working fluid in the vapor and liquid phase, and ΔPg is the hydrostatic pressure loss due to the unfavorable slopes of the device in the gravity field.

Boiling/evaporation heat transfer in capillary-porous media is very complex process. The process characteristics depend on numerous factors. Currently there is no general theoretical model, which is able to predict heat transfer parameters for different types of HTSs and working liquids. Therefore experi- mental research is the main approach to develop new enhanced HTS for Heat Loops. The results of the wick performance test carried out are presented in Figure 5. Three thermocouples have been placed in the grooves of the wick (Tgr1, Tgr2, and Tgr3), one on the foil heater attached to aluminum saddle (Theater), and one has been placed in a container with water. Maximum power was not reached due to temperature limitations of the foil heaters. But 300 W corresponds to heat flux density higher than 10 W/cm2 and there is no any evidence of vapor overheating in the grooves. The thermal resistance was 0.25 K/W (0.05, which is rather small for the given assembly, and quite lower than pristine wick without CNT (Figure 5 Supporting Information) dry out is obtained at 80 W which is much lower than with CNT. It has to be mentioned that heat flux density limit for typical nickel evaporators is around 7 W/cm2; after this value the vaporliquid interface deepens on the porous structure and significant vapor overheating can be observed. This depredates performance of LHP. It is clear that loop heat pipe thermal performance character- istics significantly depend on wick characteristics as reported by Singh et al.34 who concluded that high conductive copper wick (30 W/mK) showed superior performance than nickel wick (10 W/mK) and provided heat transfer coefficient of 26 270 W/m2K as compared to 20 700 W/m2K. The increase of wick thermal conductivity in 3 times has provided the increase of evaporation heat transfer coefficient in ∼20%. In the case of CNTs layer, the thermal conductivity of the HTS layer is increasing up to ∼60 W/mK. It allows us to expect the enhancement of evaporation heat transfer coefficient in order of 40% as compared to the standard Ni wicks that today are the most used material for commercial LHPs. On the other side, the same authors34 have reported that the heat leaks from evaporator to the compensation chamber due to heat conduction through porous matrix were larger for copper wick. With our design, we can expect much lower heat leaks because thermal conductivity of MTS ceramic porous matrix (around 0.6 W/mK) is much less than for nickel

wicks, in 50 times. Even if heat leak will not be reduced in 50 times (because the key parameter is MTS effective thermal conductivity, which is defined by empirical formulas as a ratio between thermal conductivity of working fluid and MTS porous skeleton), a significant decrease of the parasitic heat leak will be achieved. CNT detachment was not observed when the nanocomposites were immersed in a liquid under mechanical agitation (400800 rpm, 30120 min) revealing good CNT adhesion on the ceramic surface. A more aggressive treatment under sonication (50 kHz, 5 min) generated certain cloudiness in the liquid. However, SEM characterization of the sonicated nano- composites still showed a very dense covering of CNTs (Figure 6 Supporting Information). These results indicate the convenience of applying an ultrasonic treatment to the wicks before positioning them in the LHP prototype to remove the MWCNTs with less adhesion, which could be detached from the wick surface in the condensationevaporation cycles.

CONCLUSIONS

MWCNTs were grown effectively on the zircon wick surface with a good coverage. The thermal conductivity of prismatic specimens with an 8 mm length has increased in a range of 18 to 26% between 50 C and 50 C and the calculated thermal conductivity of the MWCNTs grown on the surface was 59W/mK. The effective pore diameter decreased by 42% increasing the capillary pressure in decane from 90 to 150 kPa. The increase in the contact angle in water of the zircon after growing the CNTs shows the hydrophobic character of CNTs. Measured thermal resistance of the bylayer wick was 0.25 K/W, which is rather small for the given assembly and quite lower than pristine ceramic wick. MWCNTs adhesion to the ceramic pores is strong enough to support the liquid flow through the evaporationcondensation cycles but conclusive tests have to be carried out in the prototype. The combined tuning of the surface thermal conductivity and effective pore diameter by growing CNTs makes the composite zircon-MWCNT material an alternative to monolayer wicks currently used in LHPs. The reported results show a new application of carbon nanotubes in thermal managing ’ASSOCIATED CONTENT b S Supporting Information. Images of pristine zircon wicks, after catalyst impregnation and coated with carbon nanotubes. Oven support image showing the way in which the wick is held in the boat during the growth process. Water absorption curves corresponding to the

pristine zircon wick and zircon wick coated with CNTs. Adhesion tension hysteresis cycle for ceramic zircon coated with CNTs. SEM images of CNTs over the wick after ultrasonic treatment. Experimental setup for wick thermal performance characterization and test results for the pristine zircon wick. Discussion of the configura- tions of the thermal conductivity calculation. This material is available free of charge via the Internet at http://pubs.acs.org.

AUTHOR INFORMATION

Corresponding Author

*Telephone:34976733977.

Fax:34976733318.

E-mail:mtmartinez@ icb.csic.es.

ACKNOWLEDGMENT This work was funded by the Spanish Ministry of Industry Project FIT-130500-2004-0020. M.T.M. ackcnowledge to Jesus Sanchez (Empresarios Agrupados) the useful discussions in the project planning.

REFERENCES

(1) Wong, H. S. P. Beyond the conventional transistor. IBM J. Res. Dev. 2002, 46, 133–167.

(2) Thompson, S. E.; Parthasarathy, S. Moore's law: the future of Si microelectronics. Mater. Today. 2006, 9, 20–25.

(3) Avouris, P.; Chen, Z. H.; Perebeinos, V. Carbon-based electro- nics. Nat. Nanotechnol. 2007, 2, 605–615.

(4) Choi, W. B.; Chung, D. S.; Kang, J. H.; Kim, H. Y.; Jin, Y. W.; Han, I. T.; Lee, Y. H.; Jung, J. E.; Lee, N. S.; Park, G. S.; Kim, J. M. Fully sealed, high-brightness carbon-nanotube field-emission display. Appl. Phys. Lett. 1999, 75, 3129–3131.

(5) Liu, Z.; Winters, M.; Holodniy, M.; Dai, H. J. siRNA delivery intro human T cells and primary cells with carbon-nanotube transportes. Angew. Chem., Int. Ed. 2007, 46, 2023–2027.

(6) Prato, M.; Kostarelos, K.; Bianco, A. Functionalized carbon nanotubes in drug design and discovery. Acc. Chem. Res. 2008, 41, 60–68.

(7) Freitag, M.; Tsang, J. C.; Kirtley, J.; Carlsen, A.; Chen, J.; Troeman, A.; Hilgenkamp, H.; Avouris, P. Electrically Excited, Localized Infrared Emission from Single Carbon Nanotubes. Nano Lett. 2006, 6, 1425–1433.
(8) Chen, J.; Perebeinos, V.; Freitag, M.; Tsang, J.; Fu, Q.; Liu, J.; Avouris, P. Bright infrared emission from electrically induced excitons in carbon nanotubes. Science 2005, 310, 1171–1174.
(9) Close, G. F.; Yasuda, S.; Paul, B.; Fujita, S.; Wong, H. S. P. A 1 GHz Integrated Circuit with Carbon Nanotube Interconnects and Silicon Transistors. Nano Lett. 2008, 8, 706–709.

(10) Kim, S. N.; Rusling, J. F.; Papadimitrakopoulos, F. Carbon nanotubes for electronic and electrochemical detection of biomolecules. Adv. Mater. 2007, 19, 3214–3228.
(11) Martinez, M. T.; Tseng, Y. C.; Ormategui, N.; Loinaz, I.; Eritja, R.; Bokor, J. Label-Free DNA Biosensors Based on Functionalized Carbon Nanotube Field Effect Transistor. Nano Lett. 2009, 9, 530–536.
(12) Berber, S.; Kwon, Y. K.; Tomanek, D. Unusually high thermal conductivity of carbon nanotubes. Phys. Rev. Lett. 2000, 84, 4613–4616.
(13) Hone, J. Carbon Nanotubes, Synthesis, Structure, Properties and Applications; Springer: Heidelberg, 2001.
(14) Liu, C. H.; Fan, S. S. Effects of chemical modifications on the thermal conductivity of carbon nanotube composites. Appl. Phys. Lett. 2005, 86, No. 123106/13.
(15) Nihira, T.; Iwata, T. Thermal resistivity changes in electron- irradiated pyrolitic-graphite. Jpn. J. Appl. Phys. 1975, 14, 1099–1104.
(16) Yan, X. H.; Xiao, Y.; Li, Z. M. Effects of intertube coupling and tube chirality on thermal transport of carbon nanotubes. J. Appl. Phys. 2006, 99, No. 124305.
(17) Petes, M. T.; Shi, L. Thermal and Structural Characterization of Individual Single-, Double-, and Multi-Walled Carbon nanotubes. Adv. Funct. Mat 2009, 19, 3918.
(18) Yamamoto, T.; Watanabe, K.; Hernandez, E; Mechanical properties, Thermal Stability and Heat Transport in Carbon nanotubes in Carbon Nanotubes: Springer, Berlin, Heidelberg, 2008.

(19) Xu, Z. P.; Buehler, M. J. Nanoengineering heat transfer perfomance at carbon nanotube interface. ACS Nano 2009, 3, 2767–2775.

(20) Ren, C. L.; Xu, Z. J.; Zhang, W.; Li, Y.; Zhu, Z. Y.; Huai, P. Theoretical study of heat conduction in carbon nanotube hetero- junctions. Phys. Lett. A 2010, 374 (1718), 1860–1865.

(21) Iwai, T.; Shioya, H.; Kondo, D.; Hirose, S.; Kawabata, A.; Sato, S.; Nihei, M.; Kikkawa, T.; Joshin, K.; Awano, Y.; Yokoyama, N. Thermal and source bumps utilizing carbon nanotubes for flip-chip power ampli- fiers. IEEE Int. Electron Devices Meet., Tech. Dig. 2005, 257, J;165–178.

9319 The Journal of Physical Chemistry C

(22) Chu, K.; Guo, H.; Jia, C.; Yin, F.; Zhang, X.; Liang, X.; Chen, H. Thermal Properties of Carbon NanotubeCopper Composites for Thermal Management Applications. Nanoscale Res. Lett. 2010, 5 868–874.

(23) Kordas, K.; Toth, G.; Moilanen, P.; Kumpumaki, M.; Vahakangas, J.; Uusimaki, A.; Vajtai, R.; Ajayan, P. M. Chip cooling with integrated carbon nanotube microfilm architectures. Appl. Phys. Lett. 2007, 90, No. 123105/13.

(24) Yoon, Y. H.; Song, J. W.; Kim, D. Transparent Film Heater Using Single-Walled Carbon Nanotubes. Adv. Mater. 2007, 19, 4284–4287.

(25) Wang, H.; Feng, J. Y.; Hu, X. J.; Ng, K. M. Reducing thermal contact resistance using bilayer aligned carbon nanotube thermal inter- face material. Chem. Eng. Sci. 2010, 65 (3), 1101–1108.

(26) Lin, W.; Moon, K. S.; Wong, C. P. A combined process of in situ functionalization and microwave treatment to achieve ultrasmall thermal expansion of aligned carbon nanotube polymer nanocomposites to- wards applications as thermal interface materials. Adv. Mater. 2009, 21 (23), 2421–2424.

(27) Gao, Y.; Marconnet, A. M.; Panzer, M. A.; LeBlanc, S.; Dogbe, S.; Ezzahri, Y.; Shakouri, A.; Goodson, K. E. Nanostructured Interfaces for Thermoelectrics. J. Electron. Mater. 2010, 39 (9), 1456–1462.

(28) Varshney, V.; Patnaik, S. S.; Roy, A. K.; Farmer, B. L. Modeling of Thermal Conductance at Transverse CNTCNT Interfaces. J. Phys. Chem. C 2010, 114, 16223–16228.

(29) Datye, A; Wu, K. H.; Kulkarni, S; Lin, H. T.; Vleugels, J; Li, W. Z.; Kumari, L. Aluminium nitride multi-walled nanotube (MWNTs) nanocomposite by direct in-situ growth of CNTs on Aluminum nitride particles. In Advanced processing and manufacturing technologies for structural and multifunctional materials III, 33rd International Confer- ence on Advanced Ceramics and Composites, Daytona Beach, FL, 2009; Ohji, T., Singh, M., Eds.; Wiley: Hoboken, NJ, 2010; 30 (8), pp 189204.

(30) Koszor, O; Lindemann, A; Davin, F; Balazsi, C. Observation of thermophysical and tribological properties of CNT reinforced Si3N4. In Fractography of Advanced Ceramics III, 3rd International Conference on Fractography of Advanced Ceramics, Stara Lesna, Slovakia, Sept. 710, 2008; Dusza, J., Danzer, R., Morrell, R., Quinn, G. D., Eds.; Trans Tech Publ.: Stafa-Zurich, Switzerland, 2009, Vol. 357, p 409354.

(31) Padture, N. P. Multifunctional Composites of Ceramics and Single-Walled Carbon Nanotubes. Adv. Mater. 2009, 21 (17), 1767–1770.

(32) Antoinette, P. L.; Lashmore, D. S.; Mann, J.; White, B. Adapter for thermal conduction comprises nanostructure-based conducting element and connector for maximizing number of nanostructures in contact with connector, to enable conduction between nanoscale environment/ traditional thermal circuit. Patent Number(s) WO2009021069-A1; US2009042455-A1; AU2008283846-A1; EP2176927-A1; CA2695853- A1, 2009.

(33) Riehl, R. R.; Dutra, T. Development of an experimental loop heat pipe for application in future space missions. Appl. Therm. Eng. 2005, 25, 101–112.

(34) Singh, R.; Akbarzadeh, A.; Mochizuki, M. Effect of wick characteristics on the thermal perfomance of the miniature loop heat pipe. J. Heat Trans. 2009, 131, 082601.

(35) http://www.nasatech.com/Briefs/Nov99/GSC14225.html.

(36) North, M. T.; Sarraf, D. B.; Rosenfeld, J. H.; Maidanik, Y. F.; Vershinin, S. High heat flux loop heat pipes. Sixth European Symposium on Space Environmental Control Systems, Noordwijk, The Netherlands, May 2022, 1997; Guyenne, T.-D., Ed.; European Space Agency: 1997; SP-400, p 371.

(37) Natividad, E.; Castro, M.; Burriel, R.; Angurel, L. A. Thermal conductance measurements of superconductivity Bi-2212 rods and Bi 2212-based current lead modules. Analysis and results. J. Therm. Anal. Calorim. 2006, 84, 307–316.
(38) Washburn, E. W. The dynamics of capillary flow. Phys. Rev. 1921, 17, 273–283.
(39) Hozownia, D.; Kwiatkowska, I.; Hupka, J. An investigation on wetting of porous materials. Physicochem. Probl. Miner. Process 2008, 42, 251–262.
(40) Jakson, P. V.; Hunt, J. A.; Doherty, P. J. Hidrophilicity of 3-D biomaterials: the Washburn equation. J. Mater. Sci. Mater. Med. 2004, 15, 507–511.
(41) Molina, R.; Comelles, F.; Julia, M. R.; Erra, P. Chemical modifications on human hair studied by means of contact angle determination. J. Colloid Interface Sci. 2001, 237, 40–46.
(42) Juang, Z. Y.; Lai, J. F.; Weng, C. H.; Lee, J. H.; Lai, H. J.; Tsai, C. H. On the kinetics of carbon nanotube growth by thermal CVD method. Diamond Relat. Mater. 2004, 13, 2140–2146.
(43) Gonzalez-Martín, M. L.; Labajos-Broncano, L.; Janczuk, B.; Bruque, J. M. Wettability and surface free energy of zirconia ceramics and their constituents. J. Mater. Sci. 1999, 34, 5923–5926.
(44) Feng, A.; McCoy, B. J.; Munir, Z. A.; Cagliostro, D. Wettability of transition metal oxide surfaces. Mater. Sci. Eng., A 1998, 242, 50–56.
(45) Liu, H.; Zhaia, J.; Jiang, L. Wetting and anti-wetting on aligned carbon nanotube films. Soft Matter 2006, 2, 811–821.
(46) Li, H. J.; Wang, X. B.; Song, Y. L.; Liu, Y. Q.; Li, Q.; Jiang, L.; Zhu, D. B. Super-amphiphobic aligned carbon nanotube films. Angew. Chem., Int. Ed. 2001, 40 (9), 1743–1746.
(47) Feng, L.; Li, S.; Li, H.; Zhang, L.; Zhai, J.; Song, Y.; Liu, B.; Jiang, L.; Zhu, D. Super-hydrophobic surfaces: from natural to artificial. Adv. Mater. 2002, 14, 1857–1860.
(48) Dunn, P. D.; Reai, D. A. Heat Pipes; Pergamon Press: London, 1994.
(49) Weast, R. C. Handbook of Chemistry and Physics; CRC Press: Boca Raton, 1989.
(50) Yu, F. Loop Heat Pipes. Appl. Therm. Eng. 2005, 25, 635–657.

Figures

Tables

Figure 1

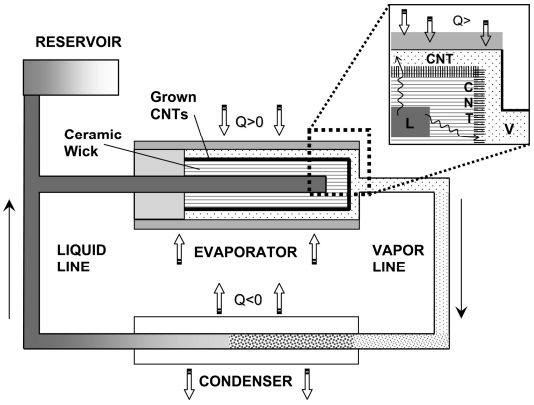

Figure 2

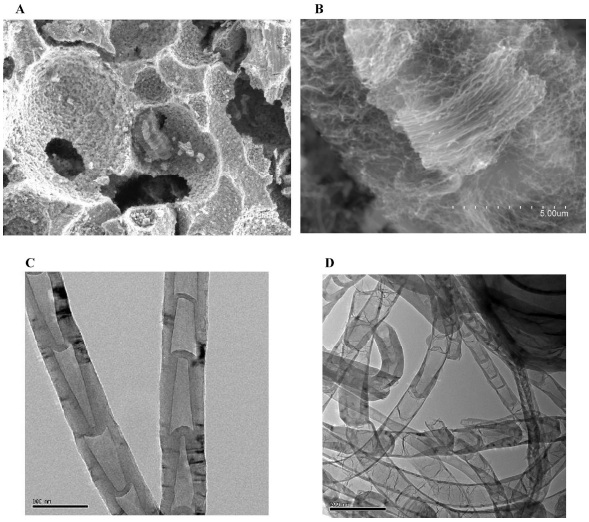

Figure 3

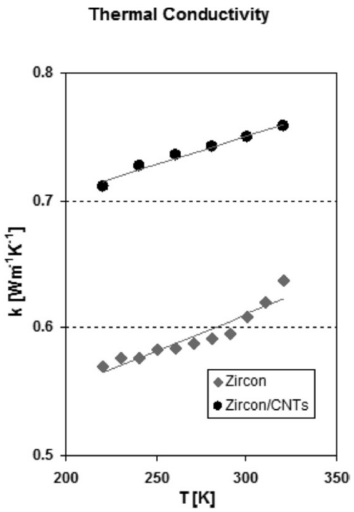

Figure 4

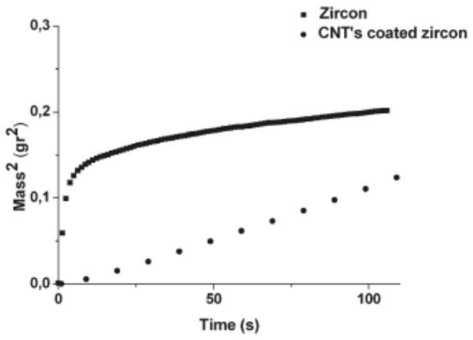

Figure 5

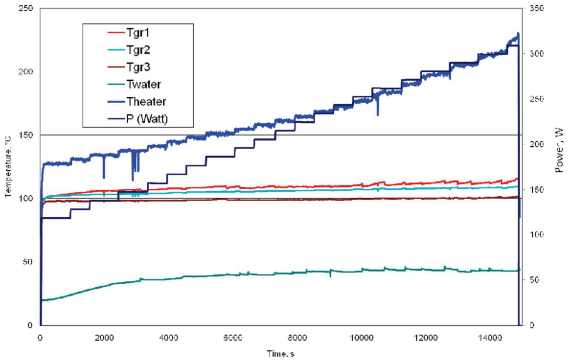

Table 1

sample	BET surface area ($m^2\ g^{-1}$)	c (cm^5)	r_{eff} (μm)
zircon	1.81	2.0×10^{-06}	0.54
CNTs coated zircon	8.52	1.1×10^{-06}	0.31